The Small Heat Shock Protein Hsp27 Affects Assembly Dynamics and Structure of Keratin Intermediate Filament Networks

Jona Kayser,[†] Martin Haslbeck,[‡] Lisa Dempfle,[†] Maike Krause,[‡] Carsten Grashoff,[§] Johannes Buchner,[‡] Harald Herrmann,[¶] and Andreas R. Bausch[†]*

[†]Lehrstuhl für Zellbiophysik, Technische Universität München, Garching, Germany; [‡]Department Chemie and Center for integrated Protein Science, Technische Universität München, Garching, Germany; [§]Group of Molecular Mechanotransduction, Max Planck Institute of Biochemistry, Martinsried, Germany; and [¶]Arbeitsgruppe Funktionelle Zellarchitektur, German Cancer Research Center (DKFZ), Heidelberg, Germany

ABSTRACT   The mechanical properties of living cells are essential for many processes. They are defined by the cytoskeleton, a composite network of protein fibers. Thus, the precise control of its architecture is of paramount importance. Our knowledge about the molecular and physical mechanisms defining the network structure remains scarce, especially for the intermediate filament cytoskeleton. Here, we investigate the effect of small heat shock proteins on the keratin 8/18 intermediate filament cytoskeleton using a well-controlled model system of reconstituted keratin networks. We demonstrate that Hsp27 severely alters the structure of such networks by changing their assembly dynamics. Furthermore, the C-terminal tail domain of keratin 8 is shown to be essential for this effect. Combining results from fluorescence and electron microscopy with data from analytical ultracentrifugation reveals the crucial role of kinetic trapping in keratin network formation.

INTRODUCTION

Heat shock proteins are essential for the cell's response to stress. They protect the cell by facilitating correct protein folding and preventing deleterious protein aggregation (1). Small heat shock proteins (sHsps), with a monomeric size ranging from 9 to 47 kDa, have been associated with processes ranging from RNA stabilization to apoptosis (2–7). Their activity can be regulated by modulating their oligomeric structure (5, 8, 9). There also is growing evidence of sHsps interacting with the cytoskeleton (10–16). This is especially interesting, since the cytoskeleton—a filamentous composite network comprised of microtubules, actin filaments, and intermediate filaments—determines the cell's mechanical properties. It therefore is a key factor for many fundamental functions and critical processes, ranging from tissue differentiation during embryogenesis to the metastatic behavior of tumor cells (17–19). Hence, precise control of the cytoskeletal architecture is of paramount importance. Although intermediate filaments are one of the primary contributors to the structural integrity of the cell, relatively little is known about how the cell governs the organization of its intermediate filament cytoskeleton. Keratins comprise the largest subgroup in the diverse intermediate filament family. They are assembled from heterodimeric coiled-coil complexes of one acidic (type I) and one basic (type II) keratin to form complex cytoplasmic networks of bundles and filaments (20). Moreover, the corresponding network morphology and substructure depend on the location of keratin within the cell: peripheral networks are generally much finer than the heavily bundled keratin structures in the perinuclear region (21,22). How the cell achieves this wealth of network substructure, however, remains largely unknown. Only a few keratin-bundling proteins—which are abundant for other cytoskeletal filaments, such as actin filaments—have so far been identified (23, 24). In a recent study, we were able to demonstrate in vitro that keratin filaments have intrinsic bundling capabilities and that the assembly dynamics has a severe impact on the resulting network structure (25). Interestingly, the small heat shock protein Hsp27 has been reported to colocalize with keratin intermediate filaments in vivo and to have an impact on the material properties of reconstituted intermediate filament gels (13). However, the underlying mechanisms of Hsp27-controlled keratin network assembly have so far not been thoroughly explored. Here, we show that Hsp27 affects the architecture of kinetically trapped keratin networks by altering their assembly dynamics. Our data demonstrate the relevance of the C-terminal keratin 8 tail domain for this effect and elucidate the underlying physics.

MATERIALS AND METHODS

Recombinant proteins

Recombinant keratins K8 and K18 were expressed, purified, and prepared as described (26). In short, proteins were expressed in *Escherichia coli*, purified, and stored in 8 M urea. Before use, basic and acidic keratins were mixed in an equimolar ratio and refolded by a stepwise dialysis to 6 M, 4 M, and 2 M urea in low-tris buffer (2 mM Tris, pH 9.0, and 1 mM dithiothreitol (DTT)). Dialysis was continued overnight into urea free buffer. Hsp27 was purified as described elsewhere and dialyzed against the same low-tris buffer to prevent any buffer-related artifacts (27). Hsp27 activity at these conditions was confirmed by investigating the suppression of the thermal aggregation of citrate synthase (CS) as a model substrate, where Hsp27 showed a half-maximal suppression at a ratio of 1:1 (CS/Hsp27), identical to reported values (28).

Tail-truncation mutants

Mutant keratins with partial or complete truncation of the C-terminal tail domain were produced by modifying the nucleotide sequence with a stop codon at the desired position. For this, a QuikChange Lightning Site-Directed Mutagenesis Kit (Agilent Technologies, Santa Clara, CA) was used according to the manufacturer's instructions. The keratin 8 tail was assumed to begin after residue 402 and that of keratin 18 after residue 388 (residue numbering inclusive of the starting methionine) (29). Additional mutants for keratin 8 were truncated after residues 426 and 466.

Fluorescent labeling

The wild-type amino acid sequence of keratin 8 does not contain any cysteines. This allows for site-specific attachment of a fluorescent marker via an introduced cysteine. For this purpose, we performed a point mutation in keratin 8, changing the native serine 243 (located in the non-α-helical L1-2 linker segment) to a cysteine using a QuikChange site-directed mutagenesis kit (Agilent Technologies). The site of the mutation was chosen such that interference of the label with protein folding is minimized. Subsequently, a fluorescent dye (ATTO647N, ATTO-TEC, Siegen, Germany) was covalently bound to the introduced cysteine according to the manufacturer's instructions. For FRET measurements, keratin 8 was labeled in the same fashion with an ATTO488 dye by an introduced cysteine at the end of the tail domain (S478C). Proper filament assembly was verified via electron microscopy. The total percentage of labeled keratin was 10% for all experiments involving fluorescent proteins (except FRET assays). Hsp27 was labeled with 5-carboxyfluorescein succinimidyl ester (5-FAM) or 5-carboxytetramethylrhodamine succinimidyl ester (5-TAMRA; Life Technologies, Carlsbad, CA) according to the manufacturer's protocol for 2 h at room temperature in PBS. Unbound label molecules were removed using a HiPrep 26/10 desalting column (GE Healthcare, Little Chalfont, United Kingdom).

Network assembly

Network assembly was initiated by adding 1:9 10-times-concentrated assembly buffer (200 mM Tris, pH 7.5, 10 mM MgCl$_2$, 2 mM CaCl$_2$, 2 mM DTT, 5 mM ATP, and 1 M KCl)/protein solution. Network assembly was carried out by droplet fusion, as described elsewhere (25). In short, a 4.5 μl droplet of protein solution is deposited on a glass coverslip and carefully merged with a 0.5 μl droplet of concentrated assembly buffer on an opposing coverslip, resulting in a disc-shaped sample of 5 μl volume with an approximate diameter of 2 mm and a height of $\sim$ 1.6 mm. Here, Hsp27 and keratin were mixed before incubation at $T = 37°$ C for ~10 min. The final pH at $T = 37°$ C was 7.3. The ATP present in the buffer serves purely to maintain conditions that are compatible with actin polymerization and does not influence Hsp27 activity (3, 4).

Fluorescence microscopy and image analysis

Confocal fluorescence microscopy was conducted on a Leica SP5 confocal microscope (Leica Microsystems, Wetzlar, Germany). All images are confocal slices taken at the sample side of assembly buffer introduction at comparable distances from the surface (160–230 μm). The network structure was verified to be homogeneous within the network volume accessible with the 63$\times$ glycerol immersion objective used in this study. The network architecture in confocal micrographs was analyzed by determining the fineness $\sigma = \xi^{-1}$. Here, ξ is defined as the characteristic length scale of the exponential distribution of the distances between neighboring structures (25, 30, 31). For assessment of the structural diversity within one sample, multiple images where taken at randomly chosen lateral positions throughout the sample (see Fig. S3 in the Supporting Material). The characteristic structure width, d, is obtained in a similar fashion by measuring the distances between the internal edges of individual structures.

For the analysis of network formation dynamics, a Fourier-analysis approach was employed. Each movie frame, associated with the time t, was subjected to a two-dimensional fastFourier transformation. The isotropic nature of the networks resulted in a radially symmetric representation in the Fourier space. We therefore applied an angular average routine, yielding the orientation-independent contribution of each spatial frequency, the structure factor $<|F(\nu)|>_\phi$. For better visualization, data were smoothed with a three-data-points rolling average.

Electron microscopy

Electron microscopy was carried out on a Phillips CM100 transmission electron microscope (Philips/FEI Corporation, Eindhoven, The Netherlands). Assembly was similar to that for samples for fluorescence imaging on a carbon-coated copper grid (Electron Microscopy Sciences, Hatfield, PA). Buffer-salt concentrations were adjusted as described in the main text. Samples where then negatively stained for visualization. The final protein concentration was 2 μM for all samples.

Analytical ultracentrifugation

To determine the sedimentation coefficient of keratin and keratin-Hsp27 complexes by sedimentation velocity experiments, we used an Optima XL-A centrifuge equipped with absorbance and interference optics (Beckman Coulter, Krefeld, Germany). All samples contained 0.77 μM of ATTO-647N-labeled wild-type keratin and optionally 77 μM of Hsp27 in 2 mM Tris, pH 9.0, and 1 mM DTT buffer. We placed 420 μL of each sample in a sapphire-capped double-sector centerpiece with a path length of 12 mm and analyzed the samples at 42,000 rpm in an eight-hole Ti-50 Beckman-Coulter rotor. Detection was performed with interference optic and absorbance optic at 647 nm to distinguish between keratin and the total protein amount. Absorbance scans were taken in the continuous scanning mode with a radial resolution of 0.003 cm and one replicate per scan. Data analysis was conducted with Sedfit (32), using a non-model-based continuous Svedberg distribution method ($c(s)$), with time and radial invariant noise enabled. Solvent density and viscosity were calculated with SEDNTERP (33).

FRET

Interaction between Hsp27 and K8/18 was monitored by fluorescence resonance energy transfer (FRET), as described elsewhere (28, 34). Keratin 8 was labeled with ATTO488 at the end of the tail region and Hsp27 was labeled with 5-TAMRA, as described above. FRET was measured by adding Hsp27-TAMRA to a constant concentration of 280 nm Keratin-ATTO488. For equilibration, the mixtures were incubated at $T = 37°$ C for 5 min (until the emission intensity stabilized) before spectra accumulation using a SPEX Fluoromax-3 fluorescence spectrometer (Jobin Yvon, Munich, Germany). The excitation wavelength was 480 nm and spectra were recorded from 500 to 650 nm. To eliminate cross-excitation contributions, emission intensities were corrected by subtracting the intensities recorded from an acceptor-only sample. Observed FRET-independent quenching of the donor was corrected with reference to a donor-only sample.

RESULTS AND DISCUSSION

In this study, we investigate the impact of Hsp27 on the network architecture of reconstituted keratin 8 (K8, type II) and keratin 18 (K18, type I) intermediate filaments. Using such an in vitro model system of the intermediate filament cytoskeleton not only enables precise control of all relevant environmental parameters, it moreover allows

for a direct assessment of the effect without secondary elements, such as protein phosphorylation, variations in gene expression, or redundancy effects of related sHsps. The colocalization of Hsp27 with keratin structures, reported in vivo, is also present in the reconstituted system (Fig. S1). This shows a direct interaction of Hsp27 with keratin filaments without the mediation of additional proteins.

Keratin filaments exhibit an intrinsic ability to interact with each other (25). In vitro they assemble into complex networks of filaments and bundles similar to those found in living cells. Although such networks are homogeneous on a mesoscopic length scale ($>10\ \mu$m), a substantial degree of bundling and clustering dominates the network's microscopic morphology (Fig. 1 a). These microscopic architectural features define the mechanical properties of the macroscopic network. It therefore is interesting to observe a pronounced alteration of the network's morphology when it is assembled in the presence of Hsp27 (Fig. 1, b–d). The perceived fineness of the network increases significantly. Moreover, the microscopic substructure appears less clustered and more regular. The strength of the effect depends on the molar ratio, R, of monomeric Hsp27 concentration, c_{27}, to monomeric keratin concentration, c_K. Assuming a native form of Hsp27 composed of ~ 16 subunits and $\sim 16 - 20$ molecules per keratin-filament cross section, R also roughly represents the ratio of Hsp27 oligomers to longitudinal filament-subunit repetition (5, 26). To evaluate this effect in a more quantitative fashion, we determine the fineness, σ, of the network, with $\sigma = \xi^{-1}$, where ξ is the characteristic distance in the network, by digital image analysis (see Materials and Methods for details). The gathered data reveal a monotonic increase of σ as a function of R over the range of Hsp27 concentrations examined, as shown in Fig. 1 e. Interestingly, even small amounts of Hsp27 ($R = 0.5$) are sufficient to have a measurable effect on the network structure. In addition to the Hsp27-induced increase in fineness, we observe less clustering and a more homogeneous network structure throughout the sample. This observation is underlined by a reduction of the characteristic structure width, d, suggesting a lesser degree of bundling and clustering in the network substructure with increasing R (Fig. 1 f).

Due to the method of sample preparation, there are regions of faster and slower network assembly in one sample (25). Interestingly, the observed Hsp27 effect is more pronounced where network formation is fast. The key to the Hsp27-induced differences in network structure might therefore be found in the details of the network's assembly dynamics. To investigate this in more detail, we assess the network formation process in real time. Within the first second after initiation of assembly, a dense arrangement of small structures emerges from the fluorescent background (Fig. 2 a and Movie S1). These structures then continuously grow and get more defined to result in a networklike array (Fig. 2, b and c). On a longer timescale, these structures then undergo a coarsening process of continued cluster
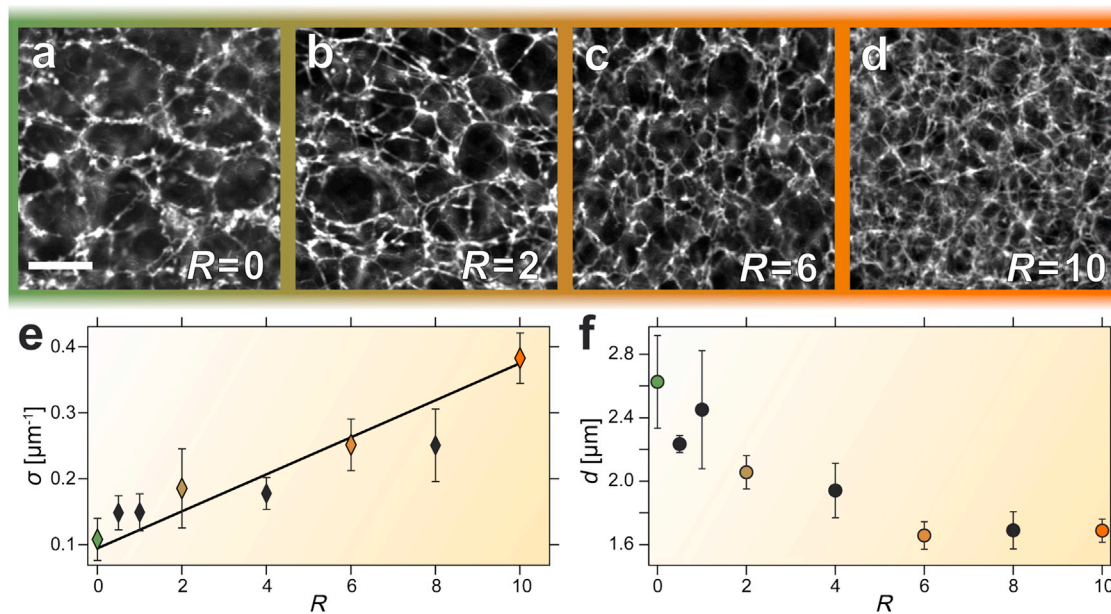

FIGURE 1 Hsp27 causes an alteration of keratin network structure. (a) In the absence of Hsp27, keratin intermediate filaments assemble into heterogeneous networks of clusters and bundles. (b–d) The presence of Hsp27 during assembly leads to a finer, more homogeneous network morphology. The strength of the effect depends on the molar ratio, R, of Hsp27 to keratin, as denoted in the figure and illustrated by the color gradient from green ($R = 0$) to orange ($R = 10$). (e) The network fineness, σ (see main text and Materials and Methods for details), monotonically increases with growing R. The linear fit to the data (*black line*) is associated with a correlation coefficient of $r = 0.86$. (f) The characteristic structure width, d, decreases with increasing R. All error bars are the mean $\pm$ SD of data from multiple images acquired at different locations in the sample. The keratin concentration was $c_K = 8\ \mu$M for all samples. All images are confocal slices. The scale is the same for all images. Scale bar, 10 μm. To see this figure in color, go online.
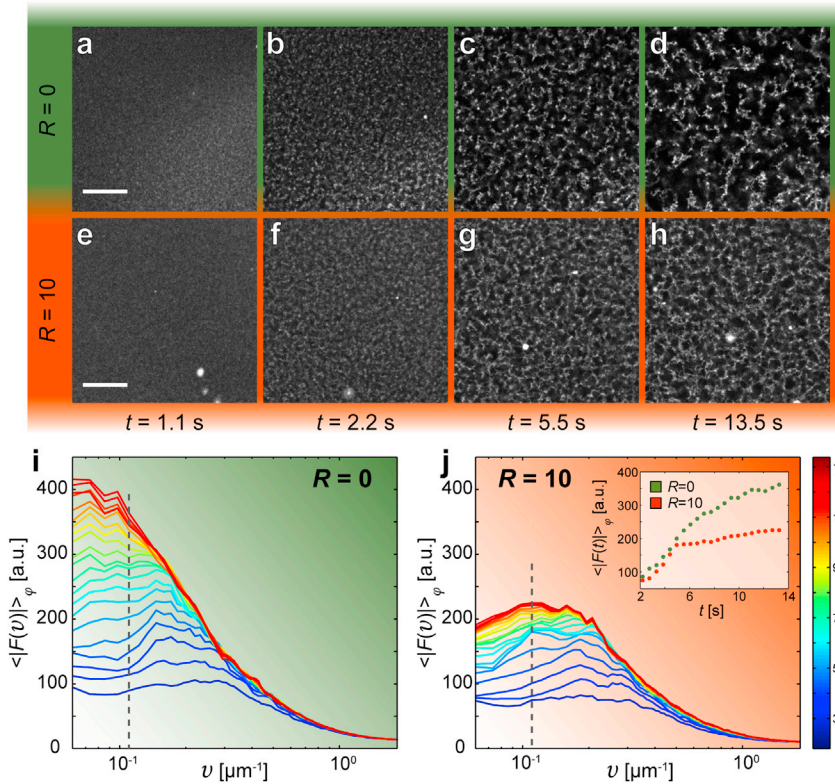
FIGURE 2 Hsp27 inhibits cluster association and network coarsening. (*a–d*) During network assembly, small nascent structures can associate to larger clusters, leading to a coarsening of the network structure. (*e–h*) The presence of Hsp27 inhibits this process, resulting in a finer network (see also Movie S1). (*i*) This difference is reflected in the time evolution of the structure factor $<|F(\nu)|>_{\phi}$, where ν is the spatial frequency. For $R = 0$, a characteristic shift to lower spatial frequencies (i.e., lower fineness) with time is observed (*blue*, ≈ 1 s; *red*, ≈ 13 s). (*j*) This shift is less pronounced for a sample with $R = 10$. Here, the coarsening comes to a halt much earlier than for the sample with $R = 0$. This is also emphasized by evaluating the temporal evolution of the structure factor for a fixed ν (*inset*). Here, $<|F(\nu)|>_{\phi}$ is shown for $\nu = 0.11$ μm^{-1} (*dashed lines* in *i* and *j*). $t = 0$ is defined by the onset of visible network formation. The keratin concentration was $c_K = 8$ μM for all samples. All images are confocal slices. The scale is the same for all images. Scale bars, 20 μm. To see this figure in color, go online.

association until they finally reach a quasistatic state (Fig. 2 *d*). Although the first phase of assembly of a sample with $R = 10$ is very similar to that of an Hsp27-free sample, the coarsening dynamics in the second phase is significantly suppressed, resulting in a much finer final network (compare Fig. 2, *a–d*, to Fig. 2, *e–h*). Here, a direct extraction of the fineness, as employed earlier, is unfeasible due to the very low signal/noise ratio in the early stage of assembly. However, to assess the evolution of the system's spatial configuration, the 2-dimensional Fourier transformation yields valuable information, as represented by the structure factor, $<|F(\nu)|>_{\phi}$ (see Materials and Methods for details). $<|F(\nu)|>_{\phi}$ is a measure of the contribution of periodic structures with a wavelength $\lambda = \nu^{-1}$. Fig. 2, *i* and *j*, shows $<|F(\nu)|>_{\phi}$ for images taken at different times during the assembly for $R = 0$ and $R = 10$, respectively.

The emergence of the network structure is reflected by a peak at $\nu \approx 0.2$ μm^{-1}. The peak then becomes increasingly pronounced as the network gets more defined. The successive increase of $<|F(\nu)|>_{\phi}$ at smaller ν is a fingerprint of the observed coarsening. This coarsening is much less pronounced in the presence of Hsp27 (Fig. 2 *j*). The time course of the assembly can be visualized by plotting the temporal evolution of the structure factor for a fixed spatial frequency. The inset in Fig. 2 *j* shows $<|F(\nu)|>_{\phi}$ for $\nu = 0.11$ μm^{-1}, corresponding to the fineness of a fully assembled network (see Fig. 1, $R = 0$). For the reference sample ($R = 0$), $<|F(\nu)|>_{\phi}$ increases continuously until saturating at $t > 13$ s, indicating a halt of assembly dynamics.

For $R = 10$, however, this halt is already observed at $t \approx 5$ s, after which no significant change in the structure factor—and hence the network morphology—is observed.

To make the effect more prominent, it might be of avail to reduce the bundling tendencies by lowering the ionic strength. However, fluorescence microscopy is not suited for observations on the sub-bundle length scales necessary to properly investigate the resulting loosely bundled networks. Here, transmission electron microscopy (TEM) allows access to the relevant length scales. In the absence of Hsp27, keratin filaments associate to bundles in a buffer with 3 mM $MgCl_2$ as the only salt (Fig. 3 *a*). If, however,
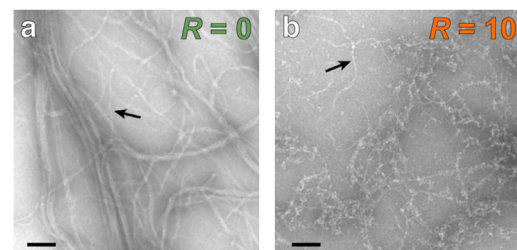

FIGURE 3 Hsp27 inhibits bundling. (*a*) In a buffer of low ionic strength (3 mM $MgCl_2$), keratin filament interaction is partially hampered, and relatively thin bundles are observed via TEM. (*b*) If Hsp27 is present ($R = 10$) during the assembly, bundles are no longer observed. Instead, single filaments, decorated by Hsp27 oligomers, are detected. The black arrows indicate single ~10-nm-wide filaments. In the absence of salt, no bundles are formed and only single filaments are observed (Fig. S5). Scale bars, 100 nm. To see this figure in color, go online.

assembly is conducted in the presence of Hsp27 ($R = 10$), bundles are no longer observed. Instead, we find single filaments, heavily decorated with characteristic ~ 10-nm-wide Hsp27 oligomers (Fig. 3 b) (35). This is reminiscent of the reported association of αB-crystallin and desmin filaments, which are critical in the context of desmin-related myopathies (10,15).

Filament elongation without bundling can be triggered by a change in pH. This can be used to temporally separate both processes (25). Adding Hsp27 to a sample with preformed filaments while bundling is simultaneously triggered by the addition of salt results in a much less pronounced impact of Hsp27 (Fig. S2). Hence, the influence of Hsp27 seems strongest in the early phases of assembly, where filament elongation is concurrent with bundling. This raises the question of whether Hsp27 has already bound to the soluble tetrameric keratin complexes before assembly is initiated or whether it exclusively interacts with assembled keratin filaments.

Analytical ultracentrifugation reveals a preassembly association of Hsp27 with soluble K8/K18 tetramers (Fig. 4). In this sedimentation velocity assay, only keratin is fluorescently labeled. In the absence of Hsp27, a characteristic tetrameric peak at a sedimentation coefficient of $s \approx 4.6$ S is observed, corroborating reported values (36). The small peaks at ~2.5 S and 8 S in the keratin-only sample are most likely monomers and octamers, respectively. Upon addition of Hsp27 a drastic decrease of the tetrameric peak can be observed, whereas a broad substrate peak, indicating a multitude of interaction species, appears at higher s-values (10–30 S). These findings indicate an interaction of keratin and Hsp27 in the preassembly phase. This is also supported by FRET measurements (Fig. 4, inset). Here, TAMRA-labeled Hsp27 (emission wavelength, $\lambda_{em} = 579$ nm) is
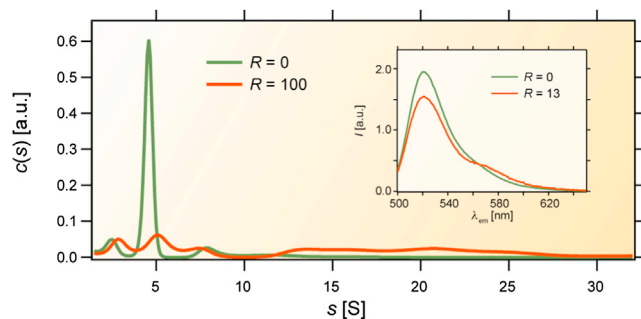
FIGURE 4 Hsp27 interacts with soluble keratin tetramers. Sedimentation velocity analytical ultracentrifugation was carried out for a sample of keratin only (green) and a sample containing keratin and Hsp27 (orange, $R = 100$). The fluorescence signal of keratin at 647 nm was detected. The strong peak at $s \approx 4.6$ S for the Hsp27 free sample is characteristic for tetrameric complexes. The peaks at s-values of 2.5 S and 8 S most likely correspond to monomeric and octameric forms of keratin. The peak at 5 S diminishes in the presence of Hsp27 and is replaced by a broad substrate peak ranging from 10 S to 30 S, indicating multiple interaction species. (Inset) FRET spectra of ATTO488-labeled keratin (donor; $\lambda_{em} = 523$ nm) in the absence and presence of TAMRA-labeled Hsp27 (acceptor; $\lambda_{em} = 579$ nm). To see this figure in color, go online.

showing a FRET signal in the presence of ATTO488-labeled keratin (excitation at $\lambda_{ex} = 480$ nm, $\lambda_{em} = 523$). The label is attached to the end of the K8 tail domain, suggesting that this is the location of keratin-Hsp27 interaction.

To unravel the physical basis for the impact of Hsp27 on keratin network assembly, it is crucial to better understand how both players interact. The bundling capabilities of keratin intermediate filaments have been tentatively attributed to an interaction via their C-terminal tail domains. These unstructured domains protrude from the filament surface and have for certain keratin types been demonstrated to be essential for bundling (37). Therefore, the tail domain of K8, K18, or both might well be of significance for the Hsp27-induced alteration in the keratin network architecture. To investigate the role of the tail domains for the Hsp27 effect, we examine mutants of K8 and K18 where the C-terminal domain has been deleted. Here, it should be kept in mind that with a length of 81 amino acids, the tail of K8 is almost twice as long as the K18 tail (42 amino acids). Comparing the effect of Hsp27 on the network architecture of tailless mutants (K8ΔT and K18ΔT) with that observed for the wild-type confirms the hypothesized relevance of the tail region: whereas the K18ΔT mutant exhibits an increase in fineness comparable to that of the wild-type (Fig. 5, a and b), the truncation of the K8 tail
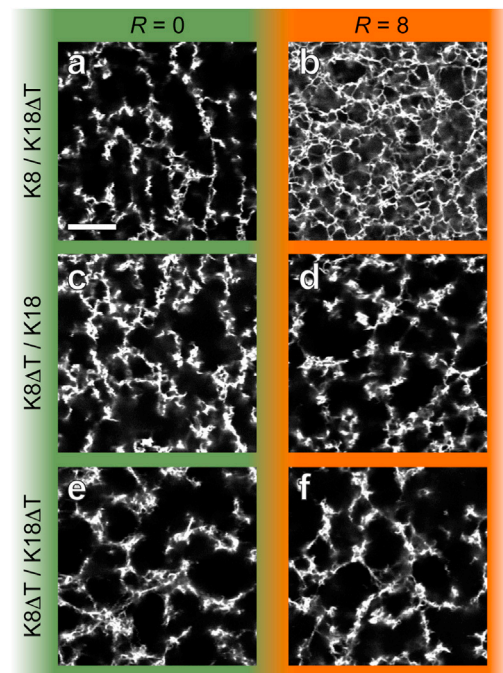
FIGURE 5 The K8 tail is crucial for the Hsp27-effect. Different combinations of wild-type proteins and tailless mutants are assessed. (a and b) The combination K8/K18ΔT shows the same characteristic increase in fineness as observed for the wild-type. (c–f) K8ΔT/K18, however, shows no susceptibility to Hsp27 at all, and this also holds true for K8ΔT/K18ΔT (e and f). The keratin concentration was $c_K = 6$ μM for all samples. All images are confocal slices. The scale is the same for all images. Scale bar, 10 μm. To see this figure in color, go online.

virtually eliminates the Hsp27 effect (Fig. 5, *c* and *d*). Combining both mutants, so that neither K8 nor K18 features a tail domain, also renders the sample insensitive to Hsp27 (Fig. 5, *e* and *f*). We note that deleting the tails also has an influence on the general network structure in the absence of Hsp27. This observation underlines the notion of the tail domains mediating filament-bundling interactions. However, as bundling is still observed for networks of K8ΔT/K18ΔT, the bundling propensity of keratins appears more convoluted than tail-mediated attraction alone.

Having established the necessity of the K8 tail for Hsp27 to unveil its full impact, we now aim to dissect the tail in a more controlled fashion. Since bundling only occurs in buffers of significant ionic strength, the tail's charge distribution might well be an important factor for bundling and keratin-Hsp27 interaction. Especially considering the characteristic charge distribution of the K8 tail domain, the C-terminal quarter of the tail features both acidic and basic amino acids, with an overall negative charge at physiological pH. The rest of the tail has an exclusively positive charge (Fig. 6, *inset*). Using a series of K8 mutants with partial tail truncations, we study the influence of different regions in the K8 tail domain on the effect of Hsp27. With reference to the charge distribution, we truncate the tail after residue 466, eradicating the negatively charged part (K8ΔT$_{466}$, length of the tail reduced to 79% with respect to that of the wild-type). A second mutant (K8ΔT$_{426}$) reduces the tail to 30% of its original length. Both mutants alter the Hsp27 effect. Surprisingly, the K8ΔT$_{466}$ variant exhibits an even stronger susceptibility to Hsp27 than

does the wild-type. The fineness at $R = 4$ is increased by more than a factor of 3, as opposed to a factor of ≈ 1.7 in the case of the wild-type (Fig. 6). K8ΔT$_{426}$, on the other hand, shows no significant change in fineness, similar to the complete tail truncation.

In a recent study, we were able to demonstrate that K8/K18 intermediate filaments form kinetically trapped, out-of-equilibrium networks in vitro (25). The architecture of such networks is determined by their assembly dynamics. The key feature of these network is the competition between filament elongation and lateral association during network formation (Fig. 7, *no Hsp27*): In the early stages of assembly, short filaments can diffuse and laterally associate to bundles and clusters of bundles. However, longitudinal growth of filaments and bundles eventually leads to a percolating, quasistatic state of the network where lateral diffusion is suppressed and hence further lateral growth is inhibited. Shifting the balance from lateral to longitudinal growth therefore leads to an earlier onset of this kinetic trapping and consequently a finer network structure. We argue that this concept is the basis for the impact of Hsp27 on the keratin network structure and that the results presented here, assuming only one mode of lateral filament and bundle interaction on all length scales, converge toward one scenario (Fig. 7, *with Hsp27*): Hsp27 associates with keratin in a prefilamentous state, as verified by analytical ultracentrifugation (Fig. 4). This leads to an inhibition of lateral association of nascent filaments in the early phase of assembly, hampering bundle formation and thereby amplifying the dominance of longitudinal elongation as the favored mode of growth. As a result, a kinetically trapped state is reached much earlier and further coarsening is inhibited (Fig. 2). The decrease of the bundling rate, and with it the strength of the effect, directly depends on the amount of Hsp27 bound and hence on R (Fig. 1). Our data furthermore show that the tail of keratin 8 is essential for the observed increase in network fineness (Fig. 5). Deleting the negatively charged C-terminal part of the tail drastically enhances the effect, suggesting that electrostatics play an important role in the keratin-Hsp27 interaction (Fig. 6). Considering the overall negative charge of Hsp27 at the given buffer conditions, we speculate that electrostatic repulsion of the negatively charged distal part, in conjunction with steric hindrance, partially diminishes the attraction toward the positively charged proximal region of the tail. The scenario illustrated in Fig. 7 is very analogous to those proposed for kinetically trapped actin networks, suggesting that such mechanisms are of general importance in the context of cytoskeletal networks (38, 39).
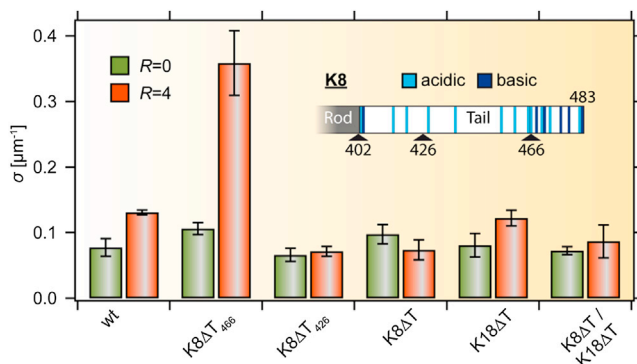

FIGURE 6 Comparison of the Hsp27-effect for different K8 tail configurations. For various tail truncation mutants, as explained in the main text, the fineness, σ, for $R = 0$ (*green*) and $R = 4$ (*orange*) is shown. Error bars indicate the mean $\pm$ SD of data from multiple images acquired at different locations in the sample. The keratin concentration was $c_K = 6$ μM for all samples. For networks of K8ΔT$_{466}$, samples with $R > 4$ exhibit a fineness that exceeds the limits of the evaluation methods; thus, the comparison is limited to samples with low R. (*Inset*) Charge distribution of the K8 tail as calculated from the amino acid sequence for pH 7.5. The truncation sites are indicated by black triangles. See Fig. S4 for confocal images of K8ΔT$_{426}$ and K8ΔT$_{466}$. To see this figure in color, go online.

CONCLUSION

This study presents evidence for a potential regulatory role of Hsp27 in the keratin cytoskeleton. Interestingly, it is
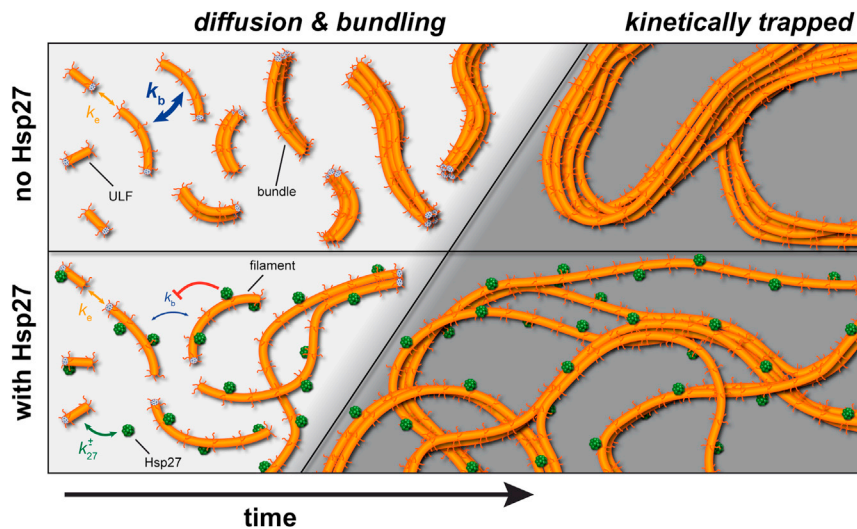
FIGURE 7 Kinetic trapping and Hsp27 influence on keratin network formation. Filaments elongate via the longitudinal annealing of unit-length filaments (*ULF*) with an elongation rate k_e. At the same time, short filaments can diffuse and laterally associate with a bundling rate k_b (*light gray region*). Here, k_e and k_b describe the general kinetics of the associated process and should not be confused with constant interaction rates of the subunits. It is the competition of these two processes, i.e., the ratio of the rates, that determines the onset of kinetic trapping (*dark gray region*) and therefore the final network structure. Binding of Hsp27, depending on its concentration and its affinity to keratin, $k_{27}^{\pm}$, hinders filament bundling (*red suppression arrow*) and results in a finer network, due to an earlier onset of kinetic trapping. To see this figure in color, go online.

not only the influence of the associated protein but the nonequilibrium nature of the network itself that is at the heart of this effect. It is, however, likely that the observed processes are much more convoluted in the setting of a living cell. The oligomeric state of Hsp27, e.g., is changed during heat shock and can be altered by phosphorylation (5). It seems probable that such changes feed back on Hsp27's effect on keratin networks. Moreover, the proximal part of the tail domain, where Hsp27 appears to bind, features one of K8's major phosphorylation sites. Future work will therefore have to investigate how keratin phosphorylation affects Hsp27-keratin interaction. We note that in many cancer types, Hsp27 overexpression correlates with increased metastatic capabilities of malignant tumor cells (40). In addition, recent studies report an increased tumor cell migration due to SPC-induced reorganization of the keratin cytoskeleton (22, 41, 42). It will therefore be exciting to further explore the role of Hsp27-dependent alterations of the keratin cytoskeleton in vivo. The networks investigated in this work, even at high Hsp27 concentrations, still exhibit relatively large mesh sizes compared to those found in cells (43). Although such fine networks can also be produced in vitro—e.g., by increasing protein concentration—the associated length scales are below the resolution of a standard confocal microscope, calling for more advanced techniques, such as stimulated emission-depletion (STED) microscopy. Future work will furthermore address the challenges of rheological assessment of keratin bundle networks, until now unfeasible due to the complexity of sample preparation. Kinetic trapping has also been reported for reconstituted actin-bundle networks, underlining the significance of such mechanisms for the formation of cytoskeletal networks (38, 39, 44). Thus, the next steps will be toward using a combination of reconstituted actin and keratin networks to investigate the role of kinetic trapping in such cytoskeletal composite systems.

REFERENCES

1. Richter, K., M. Haslbeck, and J. Buchner. 2010. The heat shock response: life on the verge of death. *Mol. Cell.* 40:253–266.

2. Haslbeck, M., T. Franzmann, …, J. Buchner. 2005. Some like it hot: the structure and function of small heat-shock proteins. *Nat. Struct. Mol. Biol.* 12:842–846.

3. Basha, E., H. O'Neill, and E. Vierling. 2012. Small heat shock proteins and α-crystallins: dynamic proteins with flexible functions. *Trends Biochem. Sci.* 37:106–117.

4. Vos, M. J., J. Hageman, …, H. H. Kampinga. 2008. Structural and functional diversities between members of the human HSPB, HSPH, HSPA, and DNAJ chaperone families. *Biochemistry.* 47:7001–7011.

5. Ehrnsperger, M., H. Lilie, …, J. Buchner. 1999. The dynamics of Hsp25 quaternary structure. Structure and function of different oligomeric species. *J. Biol. Chem.* 274:14867–14874.

6. Nover, L., K. D. Scharf, and D. Neumann. 1989. Cytoplasmic heat shock granules are formed from precursor particles and are associated with a specific set of mRNAs. *Mol. Cell. Biol.* 9:1298–1308.

7. Mehlen, P., K. Schulze-Osthoff, and A. P. Arrigo. 1996. Small stress proteins as novel regulators of apoptosis. Heat shock protein 27 blocks Fas/APO-1- and staurosporine-induced cell death. *J. Biol. Chem.* 271:16510–16514.

8. Braun, N., M. Zacharias, …, S. Weinkauf. 2011. Multiple molecular architectures of the eye lens chaperone αB-crystallin elucidated by a triple hybrid approach. *Proc. Natl. Acad. Sci. USA.* 108:20491–20496.

9. Van Montfort, R., C. Slingsby, and E. Vierling. 2001. Structure and function of the small heat shock protein/α-crystallin family of molecular chaperones. *Adv. Protein Chem.* 59:105–156.

10. Houck, S. A., A. Landsbury, …, R. A. Quinlan. 2011. Multiple sites in αB-crystallin modulate its interactions with desmin filaments assembled in vitro. *PLoS ONE.* 6:e25859.

11. Miron, T., K. Vancompernolle, …, B. Geiger. 1991. A 25-kD inhibitor of actin polymerization is a low molecular mass heat shock protein. *J. Cell Biol.* 114:255–261.

12. Nicholl, I. D., and R. A. Quinlan. 1994. Chaperone activity of α-crystallins modulates intermediate filament assembly. *EMBO J.* 13:945–953.

13. Perng, M. D., L. Cairns, …, R. A. Quinlan. 1999. Intermediate filament interactions can be altered by HSP27 and αB-crystallin. *J. Cell Sci.* 112:2099–2112.

14. Doshi, B. M., L. E. Hightower, and J. Lee. 2010. HSPB1, actin filament dynamics, and aging cells. *Ann. N. Y. Acad. Sci.* 1197:76–84.

15. Vicart, P., A. Caron, …, M. Fardeau. 1998. A missense mutation in the αB-crystallin chaperone gene causes a desmin-related myopathy. *Nat. Genet.* 20:92–95.

16. Djabali, K., B. de Néchaud, …, M. M. Portier. 1997. αB-crystallin interacts with intermediate filaments in response to stress. *J. Cell Sci.* 110:2759–2769.

17. Kasza, K. E., A. C. Rowat, …, D. A. Weitz. 2007. The cell as a material. *Curr. Opin. Cell Biol.* 19:101–107.

18. Bement, W. M., G. I. Gallicano, and D. G. Capco. 1992. Role of the cytoskeleton during early development. *Microsc. Res. Tech.* 22:23–48.

19. Kedrin, D., J. van Rheenen, …, J. E. Segall. 2007. Cell motility and cytoskeletal regulation in invasion and metastasis. *J. Mammary Gland Biol. Neoplasia.* 12:143–152.

20. Herrmann, H., S. V. Strelkov, …, U. Aebi. 2009. Intermediate filaments: primary determinants of cell architecture and plasticity. *J. Clin. Invest.* 119:1772–1783.

21. Kölsch, A., R. Windoffer, …, R. E. Leube. 2010. The keratin-filament cycle of assembly and disassembly. *J. Cell Sci.* 123:2266–2272.

22. Busch, T., M. Armacki, …, T. Seufferlein. 2012. Keratin 8 phosphorylation regulates keratin reorganization and migration of epithelial tumor cells. *J. Cell Sci.* 125:2148–2159.

23. Coulombe, P. A., and M. B. Omary. 2002. "Hard" and "soft" principles defining the structure, function and regulation of keratin intermediate filaments. *Curr. Opin. Cell Biol.* 14:110–122.

24. Hofmann, I., C. Mertens, …, H. Herrmann. 2000. Interaction of plakophilins with desmoplakin and intermediate filament proteins: an in vitro analysis. *J. Cell Sci.* 113:2471–2483.

25. Kayser, J., H. Grabmayr, …, A. R. Bausch. 2012. Assembly kinetics determine the structure of keratin networks. *Soft Matter.* 8:8873–8879.

26. Herrmann, H., M. Häner, …, U. Aebi. 1999. Characterization of distinct early assembly units of different intermediate filament proteins. *J. Mol. Biol.* 286:1403–1420.

27. Buchner, J., M. Ehrnsperger, …, S. Walke. 1998. Purification and characterization of small heat shock proteins. *Methods Enzymol.* 290: 339–349.

28. de Miguel, N., N. Braun, …, M. Haslbeck. 2009. Structural and functional diversity in the family of small heat shock proteins from the parasite *Toxoplasma gondii. Biochim. Biophys. Acta.* 1793:1738–1748.

29. Hatzfeld, M., and K. Weber. 1990. Tailless keratins assemble into regular intermediate filaments in vitro. *J. Cell Sci.* 97:317–324.

30. Arevalo, R. C., J. S. Urbach, and D. L. Blair. 2010. Size-dependent rheology of type-I collagen networks. *Biophys. J.* 99:L65–L67.

31. Kaufman, L. J., C. P. Brangwynne, …, D. A. Weitz. 2005. Glioma expansion in collagen I matrices: analyzing collagen concentration-dependent growth and motility patterns. *Biophys. J.* 89:635–650.

32. Schuck, P. 2000. Size-distribution analysis of macromolecules by sedimentation velocity ultracentrifugation and lamm equation modeling. *Biophys. J.* 78:1606–1619.

33. Laue, T. M., B. D. Shah, …, S. L. Pelletier. 1992. Computer-aided interpretation of analytical sedimentation data for proteins. *In* Analytical Ultracentrifugation in Biochemistry and Polymer Science. S. E. Harding, A. J. Rowe, and J. C. Horton, editors. Royal Society of Chemistry, Cambridge, UK. pp. 90–125.

34. Bova, M. P., Q. Huang, …, J. Horwitz. 2002. Subunit exchange, conformational stability, and chaperone-like function of the small heat shock protein 16.5 from *Methanococcus jannaschii. J. Biol. Chem.* 277:38468–38475.

35. Ehrnsperger, M., S. Gräber, …, J. Buchner. 1997. Binding of nonnative protein to Hsp25 during heat shock creates a reservoir of folding intermediates for reactivation. *EMBO J.* 16:221–229.

36. Lichtenstern, T., N. Mücke, …, H. Herrmann. 2012. Complex formation and kinetics of filament assembly exhibited by the simple epithelial keratins K8 and K18. *J. Struct. Biol.* 177:54–62.

37. Lee, C. H., and P. A. Coulombe. 2009. Self-organization of keratin intermediate filaments into cross-linked networks. *J. Cell Biol.* 186: 409–421.

38. Falzone, T. T., M. Lenz, …, M. L. Gardel. 2012. Assembly kinetics determine the architecture of α-actinin crosslinked F-actin networks. *Nat Commun.* 3:861.

39. Falzone, T. T., P. W. Oakes, …, M. L. Gardel. 2013. Actin assembly factors regulate the gelation kinetics and architecture of F-actin networks. *Biophys. J.* 104:1709–1719.

40. Nagaraja, G. M., P. Kaur, and A. Asea. 2012. Role of human and mouse HspB1 in metastasis. *Curr. Mol. Med.* 12:1142–1150.

41. Rolli, C. G., T. Seufferlein, …, J. P. Spatz. 2010. Impact of tumor cell cytoskeleton organization on invasiveness and migration: a microchannel-based approach. *PLoS ONE.* 5:e8726.

42. Beil, M., A. Micoulet, …, T. Seufferlein. 2003. Sphingosylphosphorylcholine regulates keratin network architecture and visco-elastic properties of human cancer cells. *Nat. Cell Biol.* 5:803–811.

43. Sivaramakrishnan, S., J. V. DeGiulio, …, K. M. Ridge. 2008. Micromechanical properties of keratin intermediate filament networks. *Proc. Natl. Acad. Sci. USA.* 105:889–894.

44. Schmoller, K. M., O. Lieleg, and A. R. Bausch. 2008. Internal stress in kinetically trapped actin bundle networks. *Soft Matter.* 4:2365–2367.

Supporting Material:

The small heat shock protein Hsp27 affects assembly dynamics and structure of keratin intermediate filament networks
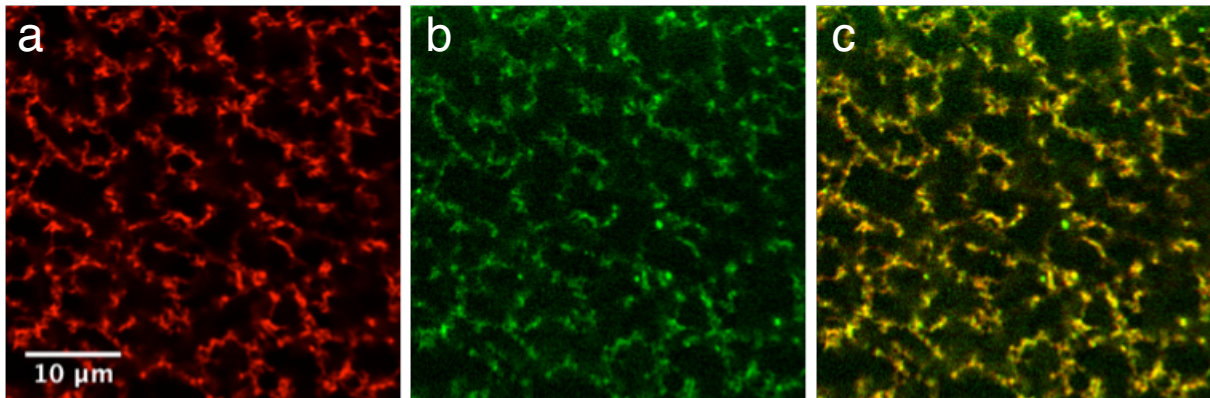

FIGURE S1 Keratin and Hsp27 colocalize in vitro. (*a*) Keratin is labeled with Atto647N . (*b*) Hsp27 is labeled with FAM. (*c*) Overlay of both channels. Channels where recorded separately and no cross excitation/emission of keratin was detected. Keratin concentration was c_K = 10 µM. The ratio of Hsp27 to keratin was R = 0.3 .
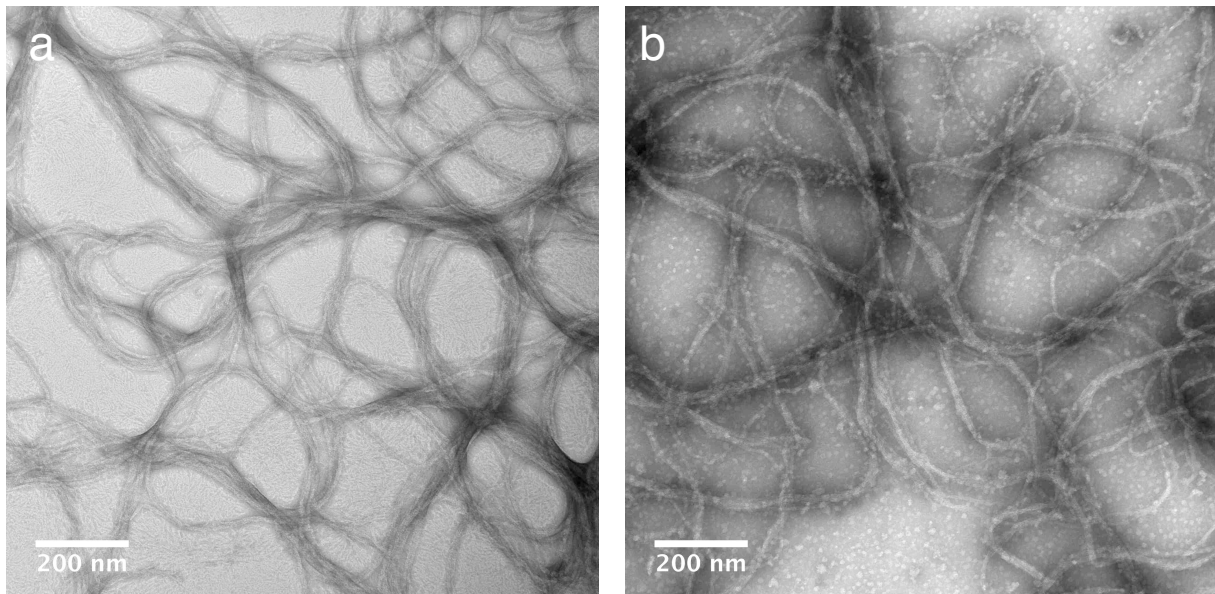

FIGURE S2 Filament elongation and bundling can be temporally separated by first assembling filaments by a drop in pH, followed by the initiation of bundling via the addition of salt (*a*). If Hsp27 is added simultaneous with the salt, after filament elongation, bundling seems to be reduced slightly (*b*). However, the effect is much less pronounced compared to Hsp27 added before initiation of filament assembly. This suggests that Hsp27 can only influence kinetic trapping in a significant manner if elongation and bundling proceed simultaneously. The protein concentration of the sample applied to the grid was c_{27} = 2 µM. All steps where carried out at room temperature.
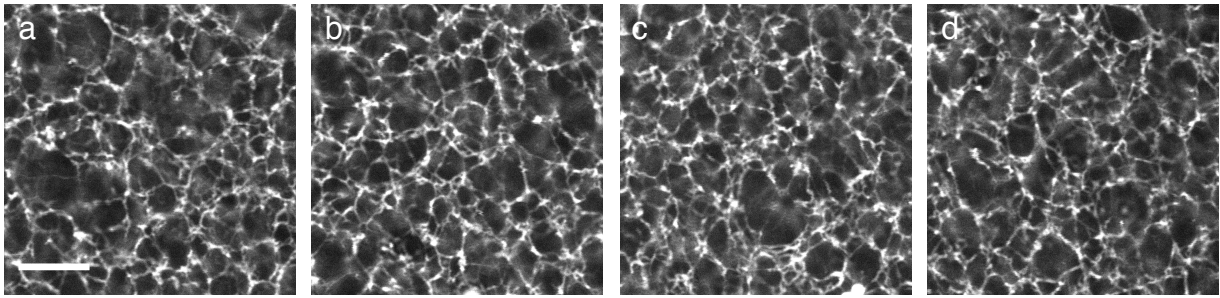
FIGURE S3 Representative confocal images taken at randomly chosen positions throughout the sample, R=6 (a-b). The standard deviation of the quantified fineness of the images can then serve as a measure for the mesoscopic homogeneity of the sample. The scale bar denotes 10 μm.
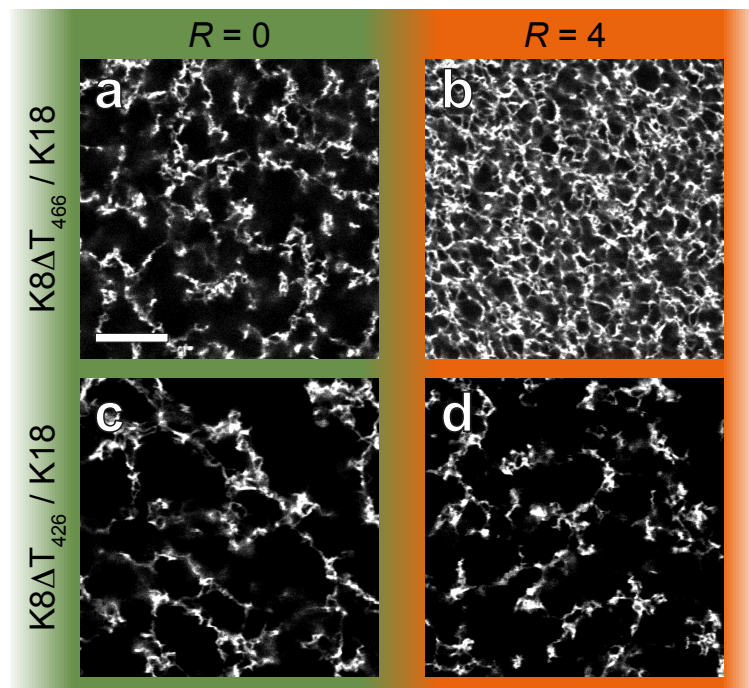

FIGURE S4 Comparison of the Hsp27 effect for the partial tail truncation mutants K8ΔT$_{466}$ (a and b) and K8ΔT$_{426}$ (c and d) . The keratin concentration was c_K=6 μM for all samples. All images are confocal slices. The scale is the same for all images. The scale bar denotes 10 μm.
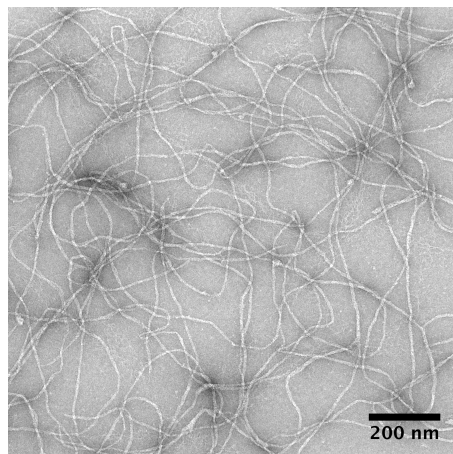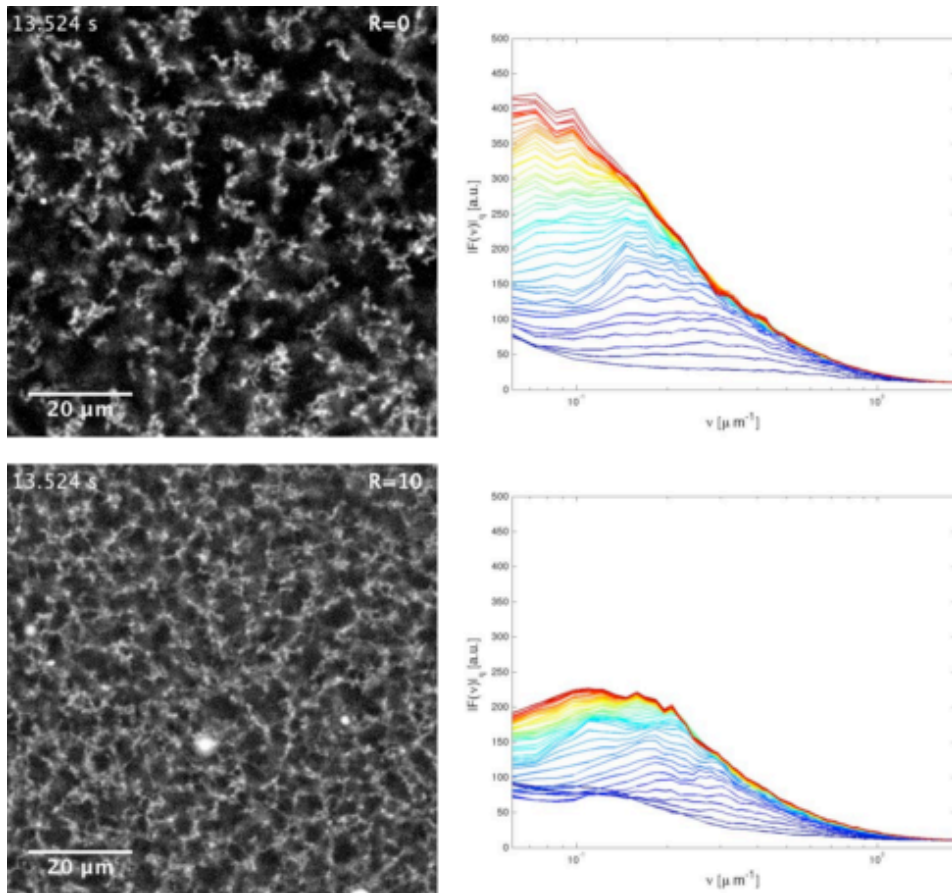

FIGURE S5 The depicted sample has a composition similar to that shown in Fig. 3a, only without salt. The image shows the expected 10 nm wide single filaments in contrast to the filament bundles in Fig. 3a.

MOVIE S1 Assembly of keratin networks (see also Fig. 2 in the main text). The movie (a still of the movie is depicted above) shows the assembly process of a keratin network without ($R=0$, top) and with Hsp27 ($R=10$, bottom). In addition to the confocal image (left) the structure factor $|F(v)|_\varphi$ is displayed (right). The corresponding time is shown in the top left corner.